PHOTONICS Research

Influences of multiphoton absorption and free-carrier effects on frequency-comb generation in normal dispersion silicon microresonators

Mulong Liu,[1,2] Leiran Wang,[1,2,*] Qibing Sun,[1] Siqi Li,[1,2] Zhiqiang Ge,[1,2] Zhizhou Lu,[1,2] Weiqiang Wang,[1,2] Guoxi Wang,[1,2] Wenfu Zhang,[1,2,3] Xiaohong Hu,[1] and Wei Zhao[1,2]

[1]State Key Laboratory of Transient Optics and Photonics, Xi'an Institute of Optics and Precision Mechanics (XIOPM), Chinese Academy of Sciences (CAS), Xi'an 710119, China
[2]University of Chinese Academy of Sciences, Beijing 100049, China
[3]e-mail: wfuzhang@opt.ac.cn
*Corresponding author: lionking@opt.ac.cn

Received 27 November 2017; revised 20 January 2018; accepted 20 January 2018; posted 23 January 2018 (Doc. ID 314400); published 22 March 2018

We investigate frequency-comb generation in normal dispersion silicon microresonators from the near-infrared to mid-infrared wavelength range in the presence of multiphoton absorption and free-carrier effects. It is found that parametric oscillation is inhibited in the telecom wavelength range resulting from strong two-photon absorption. On the contrary, beyond the wavelength of 2200 nm, where three- and four-photon absorption are less detrimental, a comb can be generated with moderate pump power, or free-carriers are swept out by a positive-intrinsic-negative structure. In the temporal domain, the generated combs correspond to flat-top pulses, and the pulse duration can be easily controlled by varying the laser detuning. The reported comb generation process shows a high conversion efficiency compared with anomalous dispersion regime, which can guide and promote comb formation in materials with normal dispersion. As the comb spectra cover the mid-infrared wavelength range, they can find applications in comb-based radiofrequency photonic filters and mid-infrared spectroscopy.

OCIS codes: (190.4380) Nonlinear optics, four-wave mixing; (190.4390) Nonlinear optics, integrated optics; (190.4970) Parametric oscillators and amplifiers; (140.3945) Microcavities.

https://doi.org/10.1364/PRJ.6.000238

1. INTRODUCTION

Microresonator-based Kerr frequency combs have attracted intense interest for their promising applications in many fields, including astronomical spectrograph calibration, high-precision frequency-comb spectroscopy, and telecommunication systems [1–4]. Such chip-level integratable microcavities with a high quality factor enable efficient nonlinear optical processes like cascaded four-wave mixing (FWM), which can lead to broadband frequency-comb generation from a continuous-wave laser. Kerr frequency combs have been observed in many platforms like MgF_2 resonators [5,6], diamond [7], silica disks [8,9], aluminum nitride [10,11], silicon nitride [12–14], and silicon [15,16], since it was first demonstrated in silica microtoroids [17]. Generally, frequency combs are generated in the anomalous dispersion region in these materials, which can be achieved by elaborate waveguide cross-section engineering. However, obtaining anomalous dispersion in an arbitrary central wavelength is still challenging, as material dispersion in the visible and near-infrared range is mostly normal due to ultraviolet absorption [12]. Moreover, materials like Si_3N_4 have a strong absorption peak near 10 μm, which will strongly influence the optical properties at shorter wavelengths [18], that is, obtaining anomalous dispersion is challenging in the mid-infrared range (MIR). Therefore, achieving Kerr frequency combs in normal dispersion materials is of particular interest, as normal dispersion is easy to access. Researchers have recently demonstrated frequency-comb and pulse generation in normal group velocity dispersion (GVD) microresonators like CaF_2 [19], MgF_2 [20], and silicon nitride [21,22]. Importantly, Xue *et al.* first reported mode-locked dark-pulse Kerr combs in normal GVD silicon nitride microresonators [23], while microcombs in normal dispersion silicon resonators have not been reported to the best of our knowledge.

Silicon is a promising candidate for an on-chip comb-generation platform since it exhibits a large nonlinear refractive index and is transparent from 2200 nm to 8500 nm without two-photon absorption (2PA), covering a significant fraction of the MIR [24]. Meanwhile, the large index contrast between

silicon and claddings (air or silicon dioxide) enables tight confinement of the optical mode, leading to a sufficiently large nonlinear coefficient and convenient dispersion engineering. One drawback to a silicon-based nonlinear process is the multiphoton absorption and concomitant free-carrier (FC) effects, which are detrimental to the efficiency of nonlinear processes. In detail, two-photon absorption is particularly strong in the telecom wavelength range, and three-photon absorption (3PA) is dominant in the range of 2200–3300 nm [25]. Considering the even longer MIR wavelength range beyond 3300 nm, four-photon absorption (4PA) and even multiphoton absorption are still present. The influences of multiphoton absorption on comb generation are of significant importance and need to be studied for future comb generation in normal dispersion silicon microresonators.

In this paper, we investigate the influences of multiphoton absorption (2PA, 3PA, and 4PA) and the accompanying FC effects over several wavelength ranges with a dual-pump regime in the normal dispersion region. It is found that 2PA is detrimental and can inhibit comb generation in the telecom wavelength range. At the MIR wavelength shorter than 3300 nm, although 3PA and the concomitant FC effects lead to the dominant nonlinear loss, a frequency comb can still be observed with a sufficiently low pump power or the FC is swept out by a positive-intrinsic-negative (PIN) structure. At longer MIR wavelengths where 4PA is dominant, a frequency comb can be generated with moderate pump power without the need for integration of a PIN diode. Interestingly, two pronounced wings of the spectra will disappear due to free-carrier effects and the duration of the generated pulses can be controlled by varying the laser detuning. The theoretical analysis is meaningful for future applications in the visible and near-IR wavelength range where material GVD is mostly normal. Meanwhile, the high conversion efficiency of the generated comb in MIR could make them candidates for comb based photonic radiofrequency (RF) oscillators and mid-infrared spectroscopy.

2. THEORETICAL MODEL

In order to model the physical process in a silicon microresonator, the Lugiato–Lefever equation including second-order dispersion, multiphoton absorption, free-carrier effects, and self-steepening is used to describe the spectral-temporal dynamics of frequency combs [26],

$$T_R\frac{\partial E(t,\tau)}{\partial t}=\left\{-\frac{\alpha}{2}-\frac{\kappa}{2}-i\delta_0+iL\frac{\beta_2}{2!}\left(i\frac{\partial}{\partial\tau}\right)^2+\left(1+\frac{i}{\omega_0}\frac{\partial}{\partial\tau}\right)\times\left[i\gamma L|E(t,\tau)|^2-\frac{\beta_{2\mathrm{PA}}L}{2A_{\mathrm{eff}}}|E(t,\tau)|^2-\frac{\beta_{3\mathrm{PA}}L}{3A_{\mathrm{eff}}^2}|E(t,\tau)|^4-\frac{\beta_{4\mathrm{PA}}L}{4A_{\mathrm{eff}}^3}|E(t,\tau)|^6\right]-\frac{\sigma L}{2}(1+i\mu)\langle N_c(t,\tau)\rangle\right\}E(t,\tau)+\sqrt{\kappa}E_{\mathrm{in}},\tag{1a}$$

$$E_{\mathrm{in}}=\sqrt{P_{\mathrm{in1}}}+\sqrt{P_{\mathrm{in2}}}\exp(-i2\pi f\tau),\tag{1b}$$

$$\frac{\mathrm{d}\langle N_c(t)\rangle}{\mathrm{d}t}=\frac{\beta_{2\mathrm{PA}}}{2\hbar\omega}\frac{\langle|E|^4\rangle}{A_{\mathrm{eff}}^2}+\frac{\beta_{3\mathrm{PA}}}{3\hbar\omega}\frac{\langle|E|^6\rangle}{A_{\mathrm{eff}}^3}+\frac{\beta_{4\mathrm{PA}}}{4\hbar\omega}\frac{\langle|E|^8\rangle}{A_{\mathrm{eff}}^4}-\frac{\langle N_c(t)\rangle}{\tau_{\mathrm{eff}}},\tag{1c}$$

where $E(t,\tau)$ is the field within the resonator, t and τ correspond to the slow time and the fast time, respectively, describing a temporal field in a single round trip at a given time t, E_{in} is the pump field with P_{in1} and P_{in2} denoting the power of two pumps, f is the frequency spacing between the two pumps, T_R is the round-trip time, L is the total cavity length, α is the round-trip loss, κ is the power transmission coefficient, δ_0 is the cavity detuning, β_2 is the second-order dispersion parameter, $\gamma=n_2\omega/cA_{\mathrm{eff}}$ is the nonlinear coefficient with n_2 the nonlinear refractive index and A_{eff} the effective mode area, $\beta_{2\mathrm{PA}}$, $\beta_{3\mathrm{PA}}$, $\beta_{4\mathrm{PA}}$ are the two-, three-, and four-photon absorption coefficients, σ is the free-carrier absorption (FCA) cross-section, and μ is the free-carrier dispersion (FCD) parameter. In Eq. (1c), the averaged FC density $\langle N_c(t)\rangle=(1/T_R)\int_{-T_R/2}^{T_R/2}N(t,\tau)\mathrm{d}\tau$ describes the buildup of carriers within the cavity over successive round trips [26]. Free-carrier generation is governed by multiphoton absorption, and the recombination rate is determined by the effective FC lifetime $\tau_{\mathrm{eff}}=5$ ns [27].

In this model, the detuning δ_0 is cavity detuning for both pumps. Theoretically, relatively small difference in detuning may lead to minor changes in comb bandwidth. We find that stable comb generation can be achieved in a large range of detuning in a dual-pump regime. So the difference in detuning will not introduce a big change of the results as long as the value of this difference is relatively small. Furthermore, the influence of different detunings can be compensated for by adjusting the frequency spacing between the two pumps. On the other hand, thermal effects have not been considered. Generally, an additional resonance shift added by thermal effects is on a much slower timescale compared to the quasi-instantaneous Kerr shift, which requires fast pump power or frequency control to stabilize the solitons. Recently, broadband soliton states can also be accessed with pump laser frequency tuning, at a rate much lower than the thermal dynamics [13]. This means that the thermal effect could affect the resonance frequency while the mode-locked state can still be achieved.

3. INFLUENCES OF TWO-, THREE-, AND FOUR-PHOTON ABSORPTION AND FC EFFECTS

In the dual-pump regime, the primary comb is generated by the low-threshold optical parametric process of nondegenerate FWM, that is, the nondegenerate FWM occurs at any pump power, avoiding the undesirable power threshold and high-power effects like stimulated Raman scattering and thermorefractive oscillations [28,29], while in the single-pump regime, degenerate FWM and intensity-dependent modulation instability process account for primary comb generation. Furthermore, a dual-pump regime for comb generation in the normal dispersion region without the need of an artificial perturbation of the local dispersion is compared to the single pump scheme.

Two-photon absorption occurring in the telecom wavelength range is first taken into account. A device with $\beta_2=0.2$ ps^2/m for normal dispersion around the pump of 1560 nm and linear loss of 1.4 dB/cm is used for simulation;

other parameters are set as follows: $\beta_{2PA} = 1.5 \times 10^{-11}$ m/W [25,30], $n_2 = 4 \times 10^{-18}$ m^2/W [31], $\kappa = 0.0172$ [32], $\sigma = 1.47 \times 10^{-21}$ m^2 [33], $\mu = 7.5$ [33], cavity radius is 100 μm, cross-sectional dimension is 500 nm × 960 nm with SiO_2 cladding, $P_{in1} = P_{in2} = 200$ mW, $f = 125$ GHz, and detuning δ_0 varies from 0 to 0.45. Figure 1(a) shows the spectra generated in the absence (blue) and presence (red) of 2PA. The spectrum bandwith without 2PA is broader than that with 2PA, signifying the significant nonlinear loss in the telecom wavelength range inhibits comb generation. When the FC effects are taken into consideration, the parametric oscillation will be totally inhibited. The corresponding temporal evolution of Fig. 1(a) (blue curve) is shown in Fig. 1(b) with the final stable flat top pulse in Fig. 1(c). It can be clearly seen that the pulse width decreases with the evolution time and finally to a stable state, which results from the increasing of detuning, that is, the pump frequency decreases, and it is red detuned to obtain the mode-locked state. This phenomenon is similar to the pulse evolution in the anomalous regime, in which the temporal width of the soliton decreases for increased detuning. The theory and measurements can be found in Refs. [34–36]. Obviously, the flat top pulse energy in the normal dispersion regime is significantly larger than that of an anomalous dispersion bright soliton.

Consequently, the nonlinear loss of 2PA in the telecom range is detrimental to frequency-comb generation, and researchers have made significant progress in comb generation at the MIR wavelength in a silicon microcavity [15,16]. In the wavelength range of 2200–3300 nm, 3PA becomes the dominant nonlinear loss process. In this section, a device with $\beta_2 = 0.2$ ps^2/m around the pump of 2400 nm and linear loss of 0.7 dB/cm is used for simulation; other parameters are set as follows: $\beta_{3PA} = 2 \times 10^{-26}$ m^3/W^2 [37], $n_2 = 7 \times 10^{-18}$ m^2/W [38], $\kappa = 0.012$, $\sigma = 4.08 \times 10^{-21}$ m^2 [39], $\mu = 4.5$ [33], cavity radius is 100 μm, cross-sectional dimension is 500 nm × 2480 nm with SiO_2 cladding, $P_{in1} = P_{in2} = 200$ mW, $f = 130$ GHz, and the detuning δ_0 is changed from 0 to 0.28. Figure 2(a) depicts the generated spectra with 3PA and FC (red), with 3PA and no FC (blue), and in the absence of 3PA (green). It can be observed that the influence of 3PA is smaller than that of 2PA in the telecom range, since the generated comb bandwidth including 3PA but no FC effects (blue) is similar to that excluding all

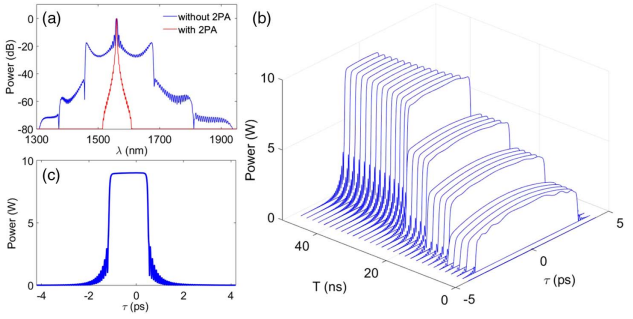

Fig. 1. (a) Frequency-comb spectra in the absence (blue) and presence (red) of two-photon absorption. (b) The corresponding temporal evolution of (a) (blue curve). (c) The final stable flat top pulse in (b).

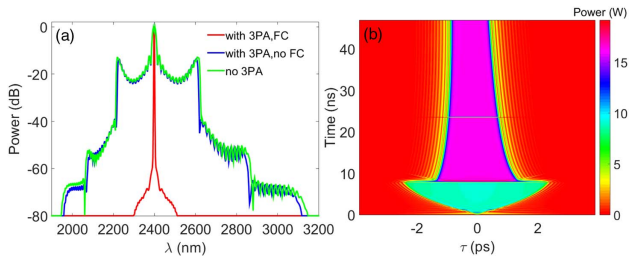

Fig. 2. (a) Spectra are generated in the presence of 3PA and FC effects (red), in the presence of 3PA without FC effects (blue), and in the absence of 3PA (green). (b) Temporal evolution of comb [blue curve in (a)] in the presence of 3PA without FC effects.

nonlinear loss terms (green). In this wavelength range, FCA becomes the dominant loss factor. It is evident that the oscillation is inhibited by FC effects (red). Moreover, the spectra are characterized by two pronounced wings (blue and green), which is in good accordance with experimental results observed in normal dispersion silicon nitride microrings [40] and magnesium fluoride resonators [20]. The corresponding temporal evolution of the spectrum including 3PA but no FC effects (blue curve) is presented in Fig. 2(b). The pulse width experiences an abrupt reduction around 10 ns, which originates from the increase of laser detuning. Finally, the temporal output evolves into a stable flat top pulse. The output spectra can be detected by a Fourier transform infrared spectrometer, and intracavity dynamics can be characterized by radio frequency (RF) modulation arising from a 3PA-induced photocurrent in experiment [16,41].

The nonlinear loss beyond 3300 nm is even lower due to the absence of 2PA and 3PA, where the dominant nonlinear loss is from 4PA. Simulation parameters are set as follows: $\beta_2 = 0.2$ ps^2/m around the pump of 4000 nm and linear loss of 0.7 dB/cm, $\beta_{4PA} = 3 \times 10^{-42}$ m^5/W^3 [25], $n_2 = 3 \times 10^{-18}$ m^2/W [27], $\kappa = 0.012$, $\sigma = 9.67 \times 10^{-21}$ m^2, $\mu = 2.9$ [27], cavity radius is 100 μm, cross-sectional dimension is 500 nm × 2760 nm with air cladding, $P_{in1} = P_{in2} = 200$ mW, $f = 135$ GHz, and the detuning δ_0 is changed from 0 to 0.11. Figure 3 shows the spectra and temporal profile with 4PA and FC effects (blue) and with 4PA without FC effects (red). It should be noted that the influence of FC effects in this wavelength range is smaller than those of 2PA or 3PA, since a comb covering more than 1000 nm can be generated in the presence of 4PA and FC

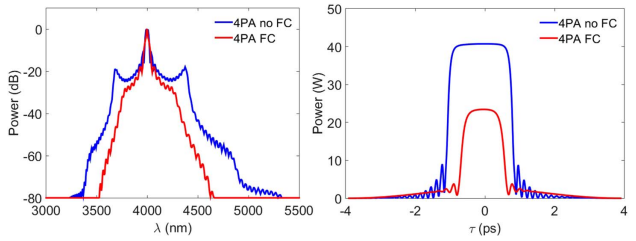

Fig. 3. (a) Spectra are generated in the presence of 4PA without FC effects (blue) and with FC effects (red). (b) Corresponding temporal profiles.

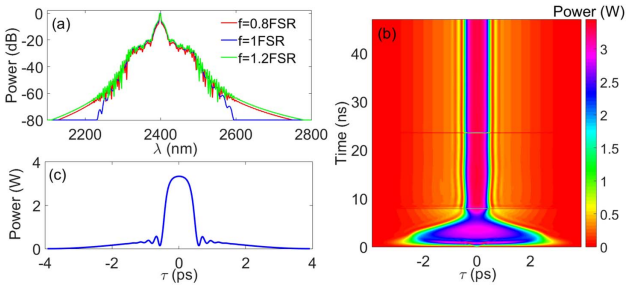

Fig. 4. (a) Spectra generated in the presence of 3PA and FC effects with different frequency separations of pumps. (b) Corresponding temporal evolution of blue curve in (a). (c) The final stable pulse of (b).

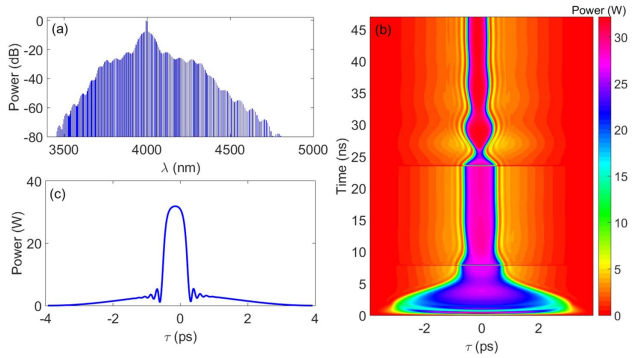

Fig. 5. (a) Spectrum generated in the presence of 4PA and FC effects. (b) Corresponding temporal evolution. (c) The final stable pulse of (b).

effects [red curve in Fig. 4(a)]. Obviously, two pronounced wings of the spectrum without FC effects disappear compared to that with FC effects in Fig. 3(a), which can be attributed to FCA. In fact, a moderate pump can avoid the detrimental FC effects in this regime, which could eliminate the integration of the PIN diode. The power ratio of the comb lines to the pump is 67% in the cavity [blue curve in Fig. 3(a)], which is more efficient than the classical anomalous dispersion regime as reported in Refs. [40,42]. A frequency comb with high-power per comb line is relevant in optical communications systems; therefore, the high-efficiency comb states in the normal dispersion regime are critical for applications in such systems.

4. MODERATE PUMP POWER FOR REDUCING FC EFFECTS AND ANALYSIS OF LASER DETUNING

It is well known that the FC generation is pump-power-dependent, and one approach to mitigate FC effects is to use lower pump power to reduce cavity circulation intensity. On account of the low-threshold dual-pump regime, the parametric oscillation can be achieved with low pump power to reduce the influence of FC effects. Figure 4 presents the results in the presence of 3PA and FC effects with a total pump power of 40 mW. In this case, pump power around 40 mW is suitable for generating a comb with the largest bandwidth. A higher power will lead to narrower comb generation due to the dominant loss from FC effects. It can be observed from Fig. 4(a) that two pronounced wings of the spectrum disappear in contrast to Fig. 2(a). This phenomenon is similar to that in Fig. 3(a) and is mainly attributed to the nonlinear loss from FCA. The temporal evolution shown in Fig. 4(b) is similar to that in Fig. 2(b). It should be noted that dispersion change due to FC effects might induce a repetition rate change of the generated pulses, which is detrimental to comb formation under the dual-pump condition. This problem can be optimized by adjusting the frequency difference of the two pumps. Theoretically, different frequency separations may introduce unequal shift of the two pumps to their corresponding resonant peaks, thus affecting the cascaded FWM efficiency and leading to change of comb bandwidth, comb lines power, and repetition rate. Spectra with varying f are shown in Fig. 4(a). In detail, we change the frequency spacing between the two pumps in the vicinity of one free spectral range (FSR). The frequency spacing can be adjusted in the range of 0.8FSR to 1.2FSR for a stable evolution and broadband comb. Furthermore, a separation of around 1.2FSR will generate a comb with the largest bandwidth in this case.

Figure 5 depicts the spectrum and temporal profile including 4PA and FC effects with total pump power of 600 mW. The spectrum in Fig. 5(a) is broader than in Fig. 4(a). The temporal pulse becomes narrower around 26 ns in Fig. 5(b), which is due to the increasing of detuning, which will introduce a small perturbation. It can be concluded that the influence of 4PA is smaller than that of 3PA, as a larger pump power can be used in the 4PA regime. In this wavelength range, a comb can be generated without the need of a PIN structure.

Interestingly, the duration of the generated flat-top pulse can be tuned continuously by varying the pump detuning. Figure 6 shows three representative results in the 4PA regime with varying detuning, and similar results can be obtained in other wavelength ranges as reported in Ref. [42]. The corresponding spectra and temporal profiles are shown in Figs. 6(a)–6(c) and 6(d)–6(f), respectively. The pulse width decreases with the increase of laser detuning, as can be seen from Fig. 6(g). A suitable detuning can lead to stable evolution of the pulse and finally to a definite pulse width. This provides a method for controlling the duration of the generated pulse by changing pump detuning.

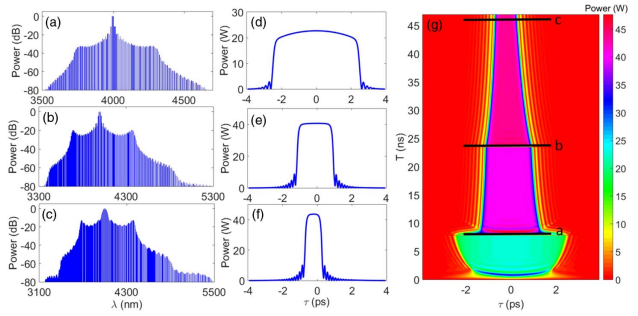

Fig. 6. (a)–(c) Spectra and (d)–(f) temporal profiles correspond to locations a, b, and c in temporal evolution of (g) with detuning of 0.05, 0.11, and 0.12, respectively.

5. CONCLUSION

In conclusion, we have investigated optical frequency-comb generation in a normal dispersion silicon microcavity with multiphoton absorption and FC effects over several wavelength ranges. Multiphoton absorption (2PA, 3PA, and 4PA) exhibits different degrees of impacts on comb generation. 2PA is particularly strong and will inhibit comb generation in the telecom wavelength range. 3PA and the generated FC lead to the suppression of parametric oscillation, while a frequency comb can also be observed when the pump power is sufficiently low or FC is swept out by a PIN structure. At longer MIR wavelengths where 4PA is dominant, a frequency comb can be generated with moderate pump power without the need of a PIN diode. The duration of the generated flat top pulses can be controlled by changing the laser detuning. These research results could promote the development of microcavity based optical frequency combs in normal dispersion media, especially in the visible and near-IR wavelength range where material GVD is mostly normal. Meanwhile, the observation of high conversion efficiency comb states is relevant to applications such as comb-based photonic RF oscillators and optical communications, which require high power per comb line.

Funding. National Natural Science Foundation of China (NSFC) (61635013, 61675231, 61475188, 61705257); Strategic Priority Research Program of the Chinese Academy of Sciences (CAS) (XDB24030600).

REFERENCES

1. T. J. Kippenberg, R. Holzwarth, and S. A. Diddams, "Microresonator-based optical frequency combs," Science **332**, 555–559 (2011).
2. A. A. Savchenkov, A. B. Matsko, and L. Maleki, "On frequency combs in monolithic resonators," Nanophotonics **5**, 363–391 (2016).
3. M.-G. Suh, Q.-F. Yang, K. Y. Yang, X. Yi, and K. J. Vahala, "Microresonator soliton dual-comb spectroscopy," Science **354**, 600–603 (2016).
4. P. Marin-Palomo, J. N. Kemal, M. Karpov, A. Kordts, J. Pfeifle, M. H. P. Pfeiffer, P. Trocha, S. Wolf, V. Brasch, and M. H. Anderson, "Microresonator-based solitons for massively parallel coherent optical communications," Nature **546**, 274–279 (2017).
5. A. A. Savchenkov, V. S. Ilchenko, F. Di Teodoro, P. M. Belden, W. T. Lotshaw, A. B. Matsko, and L. Maleki, "Generation of Kerr combs centered at 4.5 μm in crystalline microresonators pumped with quantum-cascade lasers," Opt. Lett. **40**, 3468–3471 (2015).
6. C. Y. Wang, T. Herr, P. Del'Haye, A. Schliesser, J. Hofer, R. Holzwarth, T. W. Hänsch, N. Picqué, and T. J. Kippenberg, "Mid-infrared optical frequency combs at 2.5 μm based on crystalline microresonators," Nat. Commun. **4**, 1345 (2013).
7. B. J. M. Hausmann, I. Bulu, V. Venkataraman, P. Deotare, and M. Lončar, "Diamond nonlinear photonics," Nat. Photonics **8**, 369–374 (2014).
8. S. H. Lee, D. Y. Oh, Q.-F. Yang, B. Shen, H. Wang, K. Y. Yang, Y. H. Lai, X. Yi, and K. Vahala, "Towards visible soliton microcomb generation," Nat. Commun. **8**, 1295 (2017).
9. J. Li, H. Lee, T. Chen, and K. J. Vahala, "Low-pump-power, low-phase-noise, and microwave to millimeter-wave repetition rate operation in microcombs," Phys. Rev. Lett. **109**, 233901 (2012).
10. H. Jung, C. Xiong, K. Y. Fong, X. Zhang, and H. X. Tang, "Optical frequency comb generation from aluminum nitride microring resonator," Opt. Lett. **38**, 2810–2813 (2013).
11. H. Jung, R. Stoll, X. Guo, D. Fischer, and H. X. Tang, "Green, red, and IR frequency comb line generation from single IR pump in AlN microring resonator," Optica **1**, 396–399 (2014).
12. M. Karpov, M. H. P. Pfeiffer, and T. J. Kippenberg, "Photonic chip-based soliton frequency combs covering the biological imaging window," arXiv: 1706.06445 (2017).
13. Q. Li, T. C. Briles, D. A. Westly, T. E. Drake, J. R. Stone, B. R. Ilic, S. A. Diddams, S. B. Papp, and K. Srinivasan, "Stably accessing octave-spanning microresonator frequency combs in the soliton regime," Optica **4**, 193–203 (2017).
14. L. Wang, L. Chang, N. Volet, M. H. P. Pfeiffer, M. Zervas, H. Guo, T. J. Kippenberg, and J. E. Bowers, "Frequency comb generation in the green using silicon nitride microresonators," Laser Photon. Rev. **10**, 631–638 (2016).
15. A. G. Griffith, R. K. W. Lau, J. Cardenas, Y. Okawachi, A. Mohanty, R. Fain, Y. H. D. Lee, M. Yu, C. T. Phare, and C. B. Poitras, "Silicon-chip mid-infrared frequency comb generation," Nat. Commun. **6**, 6299 (2015).
16. M. Yu, Y. Okawachi, A. G. Griffith, M. Lipson, and A. L. Gaeta, "Mode-locked mid-infrared frequency combs in a silicon microresonator," Optica **3**, 854–860 (2016).
17. I. H. Agha, Y. Okawachi, and A. L. Gaeta, "Theoretical and experimental investigation of broadband cascaded four-wave mixing in high-Q microspheres," Opt. Express **17**, 16209–16215 (2009).
18. K. Luke, Y. Okawachi, M. R. E. Lamont, A. L. Gaeta, and M. Lipson, "Broadband mid-infrared frequency comb generation in a Si_3N_4 microresonator," Opt. Lett. **40**, 4823–4826 (2015).
19. A. Coillet, I. Balakireva, R. Henriet, K. Saleh, L. Larger, J. M. Dudley, C. R. Menyuk, and Y. K. Chembo, "Azimuthal Turing patterns, bright and dark cavity solitons in Kerr combs generated with whispering-gallery-mode resonators," IEEE Photon. J. **5**, 6100409 (2013).
20. W. Liang, A. A. Savchenkov, V. S. Ilchenko, D. Eliyahu, D. Seidel, A. B. Matsko, and L. Maleki, "Generation of a coherent near-infrared Kerr frequency comb in a monolithic microresonator with normal GVD," Opt. Lett. **39**, 2920–2923 (2014).
21. X. Xue, Y. Xuan, P. H. Wang, Y. Liu, D. E. Leaird, M. Qi, and A. M. Weiner, "Normal-dispersion microcombs enabled by controllable mode interactions," Laser Photon. Rev. **9**, L23–L28 (2015).
22. S. W. Huang, H. Zhou, J. Yang, J. F. McMillan, A. Matsko, M. Yu, D. L. Kwong, L. Maleki, and C. W. Wong, "Mode-locked ultrashort pulse generation from on-chip normal dispersion microresonators," Phys. Rev. Lett. **114**, 053901 (2015).
23. X. Xue, Y. Xuan, Y. Liu, P.-H. Wang, S. Chen, J. Wang, D. E. Leaird, M. Qi, and A. M. Weiner, "Mode-locked dark pulse Kerr combs in normal-dispersion microresonators," Nat. Photonics **9**, 594–600 (2015).
24. D. C. Harris, "Durable 3-5 μm transmitting infrared window materials," Infrared Phys. Technol. **39**, 185–201 (1998).
25. X. Gai, Y. Yu, B. Kuyken, P. Ma, S. J. Madden, J. Campenhout, P. Verheyen, G. Roelkens, R. Baets, and B. Luther-Davies, "Nonlinear absorption and refraction in crystalline silicon in the mid-infrared," Laser Photon. Rev. **7**, 1054–1064 (2013).
26. T. Hansson, D. Modotto, and S. Wabnitz, "Mid-infrared soliton and Raman frequency comb generation in silicon microrings," Opt. Lett. **39**, 6747–6750 (2014).
27. R. K. W. Lau, M. R. E. Lamont, Y. Okawachi, and A. L. Gaeta, "Effects of multiphoton absorption on parametric comb generation in silicon microresonators," Opt. Lett. **40**, 2778–2781 (2015).
28. D. V. Strekalov and N. Yu, "Generation of optical combs in a whispering gallery mode resonator from a bichromatic pump," Phys. Rev. A **79**, 041805 (2009).
29. T. Hansson and S. Wabnitz, "Bichromatically pumped microresonator frequency combs," Phys. Rev. A **90**, 013811 (2014).
30. A. D. Bristow, N. Rotenberg, and H. M. van Driel, "Two-photon absorption and Kerr coefficients of silicon for 850-2200 nm," Appl. Phys. Lett. **90**, 191104 (2007).
31. M. Dinu, F. Quochi, and H. Garcia, "Third-order nonlinearities in silicon at telecom wavelengths," Appl. Phys. Lett. **82**, 2954–2956 (2003).
32. A. C. Turner, C. Manolatou, B. S. Schmidt, M. Lipson, M. A. Foster, J. E. Sharping, and A. L. Gaeta, "Tailored anomalous group-velocity dispersion in silicon channel waveguides," Opt. Express **14**, 4357–4362 (2006).

33. R. Soref and B. Bennett, "Electrooptical effects in silicon," IEEE J. Quantum Electron. **23**, 123–129 (1987).
34. T. Herr, V. Brasch, J. D. Jost, C. Y. Wang, N. M. Kondratiev, M. L. Gorodetsky, and T. J. Kippenberg, "Temporal solitons in optical microresonators," Nat. Photonics **8**, 145–152 (2014).
35. X. Yi, Q.-F. Yang, K. Y. Yang, M.-G. Suh, and K. Vahala, "Soliton frequency comb at microwave rates in a high-*Q* silica microresonator," Optica **2**, 1078–1085 (2015).
36. E. Lucas, H. Guo, J. D. Jost, M. Karpov, and T. J. Kippenberg, "Detuning-dependent properties and dispersion-induced instabilities of temporal dissipative Kerr solitons in optical microresonators," Phys. Rev. A **95**, 043822 (2017).
37. S. Pearl, N. Rotenberg, and H. M. van Driel, "Three photon absorption in silicon for 2300-3300 nm," Appl. Phys. Lett. **93**, 131102 (2008).
38. F. Gholami, S. Zlatanovic, A. Simic, L. Liu, D. Borlaug, N. Alic, M. P. Nezhad, Y. Fainman, and S. Radic, "Third-order nonlinearity in silicon beyond 2350 nm," Appl. Phys. Lett. **99**, 081102 (2011).
39. R. Claps, V. Raghunathan, D. Dimitropoulos, and B. Jalali, "Influence of nonlinear absorption on Raman amplification in silicon waveguides," Opt. Express **12**, 2774–2780 (2004).
40. X. Xue, P. H. Wang, Y. Xuan, M. Qi, and A. M. Weiner, "Microresonator Kerr frequency combs with high conversion efficiency," Laser Photon. Rev. **11**, 1600276 (2017).
41. A. G. Griffith, M. Yu, Y. Okawachi, J. Cardenas, A. Mohanty, A. L. Gaeta, and M. Lipson, "Coherent mid-infrared frequency combs in silicon-microresonators in the presence of Raman effects," Opt. Express **24**, 13044–13050 (2016).
42. G. Lihachev, M. L. Gorodetsky, T. J. Kippenberg, and V. E. Lobanov, "Frequency combs and platicons in optical microresonators with normal GVD," Opt. Express **23**, 7713–7721 (2015).